Neuregulin 1 Allosterically Enhances the Antitumor Effects of the Noncompeting Anti-HER3 Antibody 9F7-F11 by Increasing Its Binding to HER3

Christophe Le Clorennec, Hervé Bazin, Olivier Dubreuil, Christel Larbouret, Charline Ogier, Yassamine Lazrek, Véronique Garambois, Marie-Alix Poul, Philippe Mondon, Jean-Marc Barret, et al.

Neuregulin 1 allosterically enhances the anti-tumor effects of the non-competing anti-HER3 antibody 9F7-F11 by increasing its binding to HER3

Christophe Le Clorennec[1,2,3,4], Hervé Bazin[5], Olivier Dubreuil[6], Christel Larbouret[1,2,3,4], Charline Ogier[1,2,3,4], Yassamine Lazrek[1,2,3,4,8], Véronique Garambois[1,2,3,4], Marie-Alix Poul[1,2,3,4], Philippe Mondon[7,9], Jean-Marc Barret[6], Gérard Mathis[5], Jean-François Prost[6], André Pèlegrin[1,2,3,4], Thierry Chardès[1,2,3,4]

[1]IRCM, Institut de Recherche en Cancérologie de Montpellier, Montpellier, 34298, France

[2]INSERM, U1194 Montpellier, 34298, France

[3]Université de Montpellier, Montpellier, 34298, France

[4]ICM, Institut régional du Cancer de Montpellier, 34298, France

[5]CisBio SA, Le Codolet, 30200, France

[6]GamaMabs Pharma SA, Centre Pierre Potier, Toulouse, 31106, France

[7]Millegen SA, Labège, 31670, France

Running title

Non-NRG1-competing HER3 antibody hijacks ligand addiction

Present address

[8]Institut Pasteur de Guyane, 23 avenue Pasteur, BP 6010, 97306, Cayenne Cedex, France

[9]LFB Biotechnologies, 10 boulevard de Belfort, 59000, Lille, France

Keywords

Cancer, HER3, neuregulin, antibody, treatment, allostery

Financial support

This work was supported by the program “Investissement d’Avenir” (grant agreement: Labex MabImprove, ANR-10-LABX-53-01; A. Pèlegrin) and by the grant AAP13 “Fonds Unique Interministériel” FUI UmAbHER3 F120402M (T. Chardès).

Corresponding author

Dr T. Chardès, Institut de Recherche en Cancérologie de Montpellier, Montpellier, 34298, France

thierry.chardes@inserm.fr

Phone number: (33) 467 612 404

Fax number: (33) 467 613 727

Disclosure of potential conflicts of interest

O. Dubreuil, J-M. Barret and J-F. Prost are employed by GamaMabs Pharma. A. Pèlegrin, C. Larbouret and T. Chardès are inventors of the WO2012/156532 patent “Anti-human HER3 and uses thereof”, the WO2015/067986 patent “Neuregulin allosteric anti-HER3 antibody”, and the WO2016/177664 patent “Low-fucose anti-human HER3 antibodies and uses thereof”. The other authors declare no conflict of interest.

Word count: 4957

Total number of figures and tables: 6

Supplemental figures: 6

Abstract

Exploratory clinical trials using therapeutic anti-HER3 antibodies strongly suggest that neuregulin (NRG1; HER3 ligand) expression at tumor sites is a predictive biomarker of anti-HER3 antibody efficacy in cancer. We hypothesized that in NRG1-expressing tumors, where the ligand is present before antibody treatment, anti-HER3 antibodies that do not compete with NRG1 for receptor binding have a higher receptor-neutralizing action than antibodies competing with the ligand for binding to HER3. Using time resolved-fluorescence energy transfer (TR-FRET), we demonstrated that in the presence of recombinant NRG1, binding of 9F7-F11 (a non-ligand competing anti-HER3 antibody) to HER3 is increased, whereas that of ligand-competing anti-HER3 antibodies (H4B-121, U3-1287, Ab#6, Mab205.10.2 and MOR09825) is decreased. Moreover, 9F7-F11 showed higher efficacy than antibodies that compete with the ligand for binding to HER3. Specifically, 9F7-F11 inhibition of cell proliferation and of HER3/AKT/ERK1/2 phosphorylation as well as 9F7-F11-dependent cell-mediated cytotoxicity were higher in cancer cells pre-incubated with recombinant NRG1 compared with cells directly exposed to the anti-HER3 antibody. This translated *in vivo* into enhanced growth inhibition of NRG1-expressing BxPC3 pancreatic, A549 lung and HCC-1806 breast cell tumor xenografts in mice treated with 9F7-F11 compared with H4B-121. Conversely, both antibodies had similar anti-tumor effect in NRG1-negative HPAC pancreatic carcinoma cells. In conclusion, the allosteric modulator 9F7-F11 shows increased anti-cancer effectiveness in the presence of NRG1 and thus represents a novel treatment strategy for NRG1-addicted tumors.

Introduction

Retrospective analyses of clinical trials correlated the expression level of the HER3 ligand neuregulin (NRG1) with the efficacy of anti-HER3 antibodies in solid tumors (1–7). NRG1 tumor expression is not only predictive of the response to HER3 inhibitors (1,2,5,6,8–10), but could also represents a prognostic marker of cancer recurrence, as demonstrated in head and neck squamous cell carcinoma (10). HER3 expression has been associated with worse prognosis in solid tumors (11), but no clear correlation has been found between HER3 and NRG1 expression in cancer. High NRG1 expression in cancer cells (12) defines a population of tumors that may be dependent or addicted to ligand-activated signaling via HER3 and/or HER4. This autocrine loop that involves high NRG1 expression and leads to HER3 activation has been described in head and neck (10,13,14), breast (15–17), lung (18,19) and ovarian cancer (20). Activation of this loop induces resistance to EGFR- or HER2-targeted therapies (21,22) and to chemotherapy (23) that can be overcome by treatment with agents against HER3, as demonstrated in ovarian (20), colorectal (24,25), breast (26) and lung cancer (27,28). Moreover, NRG1 gene fusions have been identified as oncogenic drivers of subtypes of lung, breast and ovarian cancer (29–33) that could be indirectly targeted by HER3 inhibitors (34). Another potential role of NRG1 as a therapeutic predictive biomarker is linked to its expression in the tumor microenvironment (12). Indeed, NRG1 is secreted by cancer-associated fibroblasts and mesenchymal stem cells and subsequently, in a paracrine manner, can activate HER3 signaling, thus promoting resistance to kinase inhibitors, in melanoma (35,36), colorectal (37), gastric (38) and pancreatic cancer (39).

Most of the current efforts focus on the development of anti-HER3 agents that directly interfere with or allosterically block NRG1 binding site (40). However, these molecules have failed in phase III clinical trials (NCT02134015), possibly because in NRG1-positive tumors, the ligand is already bound to HER3 before the antibody treatment. Therefore, we hypothesized that an allosteric, non-ligand competing anti-HER3 antibody could be more effective than ligand-competing antibodies because (i) it will not need to displace NRG1 from

HER3 to be effective, and (ii) it will be more active when the ligand is already expressed in tumors. Allosteric small molecules with this particular profile have been already developed to manipulate G protein-coupled receptors (GPCRs) (41,42).

We thus generated the non-NRG1 competing allosteric anti-HER3 antibody 9F7-F11 by immunizing mice with fibroblasts that express HER2/HER3 and that were pre-stimulated with NRG1 to favor HER3 active conformation. 9F7-F11 binds specifically to HER3- or HER2/HER3-transfected fibroblasts, but not to EGFR-, HER2- or EGFR/HER4-transfected fibroblasts (43). This antibody blocks the PI3K/AKT pathway (43,44) and induces HER3 downregulation (45), leading to *in vivo* tumor regression. We now wanted to determine whether 9F7-F11 acts as a non-ligand competing allosteric modulator and modifies NRG1 activity. By using time resolved-fluorescence energy transfer (TR-FRET) we showed that 9F7-F11 binding to HER3 is enhanced by NRG1. Reciprocally, 9F7-F11 increased NRG1 binding to HER3. This translated into a better efficacy of 9F7-F11 in inhibiting NRG1-mediated cell proliferation and signaling and in promoting ADCC in tumor cells compared with NRG1-competing antibodies. Finally, as a positive modulator of NRG1 binding and negative modulator of NRG1 biological effects, the allosteric 9F7-F11 antibody reduced tumor growth of NRG1-expressing pancreatic, lung and breast cancer cell xenografts more potently than a ligand-competing anti-HER3 antibody.

Materials and methods

Cell culture

The BxPC3 and HPAC (pancreas), HCC-1806 and MDA-MB-453 (breast), and A549 (lung) human cancer cell lines were obtained from the American Type Culture Collection (ATCC) (Rockville, MD). All cell lines were free of mycoplasma contamination, determined by using the MycoAlert™ Detection Kit (Lonza, Switzerland), and were authenticated by short tandem repeat profiling using the Promega PowerPlex 21 System.

Recombinant proteins and antibodies

Recombinant human HER3 extracellular domain (ECD) and human CD16a (FcγRIIIA) were purchased from R&D Systems (Minneapolis, MN). Human recombinant NRG1-β1 ECD (all experiments) and NRG1-β3 EGF domain (Figure 1 only) were provided by R&D Systems and Millipore (Billerica, MA), respectively. The fully human H4B-121 (ligand-competing) and the mouse monoclonal 9F7-F11 (non-ligand competing) anti-HER3 antibodies (developed in our laboratory) were obtained as previously described (43). The control antibody Px is an IgG_1 monoclonal antibody purified from the mouse myeloma cell line MOPC21. The anti-HER3 antibody MAB3481 was purchased from R&D Systems, whereas Ab#6 (described in patent WO2008/100624; parental molecule of the MM-121 antibody) (46), U3-1287 (described in patent WO2007/077028; parental molecule of patritumab) (26), MOR09825 (described in patent WO2012/022814; parental molecule of the LJM716 antibody) (47), Mab205.10.2 (described in patent WO2012/022814; parental molecule of the RG7116 antibody) (48), and the chimeric antibody 9F7-F11 (ch9F7-F11) were produced as recombinant antibodies in HEK293-F cells (IgG_1 format) using the FreeStyle MAX Expression System (Invitrogen) according to the manufacturer's protocol. The low-fucose antibodies H4B-121-Emb and ch9F7-F11-Emb were produced in the YB2/0 cell line according to the Emabling® Technology developed by LFB Biomanufacturing (France). For western blotting, rabbit monoclonal

antibodies against total and phosphorylated HER3 (at Tyr1289, Tyr1197 or Tyr1222), total and phosphorylated AKT (Ser473), total and phosphorylated ERK1/2 (Thr202/Tyr204), β-actin and β-tubulin were from Cell Signaling Technology (Danvers, MA).

SNAP-tagged HER3 expression in HEK293 cells and Lumi4-Tb labeling

The Tag-lite® platform (Cisbio Bioassays, Codolet, France), which combines homogenous time resolved fluorescence (HTRF) with the SNAP-tag® technology, was used to study anti-HER3 antibodies and NRG1 binding to HER3. A Tag-lite plasmid that encodes HER3 fused to SNAP-tag® (Cisbio) was transiently expressed in HEK293 cells. At 80% confluency, the cell medium was removed and replaced by 12 ml of fresh cell culture medium. The transfection mixture [20 μl of 1μg/ml SNAP-tagged HER3 plasmid (Cisbio), 60 μl of Lipofectamine 2000 and 8 ml of Opti-MEM medium (Life Technologies Inc.)] was pre-incubated at room temperature for 20min before addition to the cells. Cells were then incubated for 24h before labeling with 200nM SNAP-Lumi4®-Terbium (Tb) substrate (Cisbio) in Tag-lite medium (Cisbio) at 37°C for 1h. After four washings, Lumi4®-Tb-SNAP-tagged HER3-expressing cells were resuspended in Tag-lite medium at a suitable density to perform TR-FRET experiments.

TR-FRET assays

One hundred microliters of 1 mg/ml anti-HER3 antibodies in pH8 phosphate buffer were labeled with the acceptor dye using the d2 Labeling Kit (Cisbio). Antibody-d2 conjugates at the optimal fluorophore/antibody ratio of 2.5 were purified on NAP5 columns (GE Healthcare, Little Chalfont, UK) in 50mM phosphate buffer, pH7. For competition experiments with unlabeled NRG1, ten-fold serial dilutions (from $4x10^{-12}$ M to $4x10^{-5}$ M) of NRG1-β1 ECD or NRG1-β3 EGF domain were prepared in Tag-lite medium. Lumi4®-Tb-SNAP tagged HER3-expressing cells were seeded in white 384-well plates at a density of 20,000 cells/10 μl/well, followed by addition of serial dilutions of competitor NRG1 (5 μl/well) and 0.5nM of anti-HER3

antibody-d2 conjugates (5 µl/well) diluted in Tag-lite medium. For the competition experiments with unlabeled anti-HER3 antibodies, five-fold serial dilutions (from $5x10^{-12}$ M to $8x10^{-7}$ M) of anti-HER3 antibodies, as competitors, were co-incubated with Lumi4®-Tb-SNAP tagged HER3-expressing cells and 12.5nM NRG1-d2 conjugate in 384-well plates. After incubation at room temperature for 5h30, the TR-FRET signal (665 nm/620 nm emission ratio) was measured on a Pherastar FS reader in Time Resolved Fluorescence mode and, normalized to 100% binding. Negative control wells contained only cells and Tag-lite buffer, whereas 100% binding was obtained by incubating antibody-d2 conjugates without NRG1, or NRG1-d2 conjugates without antibodies. The positive control for competition consisted in co-incubating serial dilutions of unlabeled NRG1 with 12.5nM NRG1-d2 conjugate (Cisbio). All experiments were done in triplicate.

HER3 and CD16a (FcγRIIIA) ELISA binding assays

Flat-bottom 96-well Maxisorp plates (Nunc, Paisley, UK) were coated with 50ng/well of recombinant human HER3 ECD, or 200ng/well of recombinant CD16a at 4°C for 18h, and then blocked with 2% BSA in phosphate-buffered saline. After washings in PBS/0.1% Tween 20 (PBS-T), anti-HER3 antibodies were added at 37°C for 1h. After washes with PBS-T, antibody binding to HER3 was detected by incubation with a horseradish-conjugated goat $F(ab')_2$ antibody against human $F(ab')_2$ (Jackson Immunoresearch, West Grove, PA) at 37°C for 2h. For the CD16a ELISA assay, anti-HER3 antibodies were pre-incubated with the horseradish-conjugate (Jackson Immunoresearch) at room temperature for 1h, before addition to the CD16a-coated plates at 37°C for 1h. After three washes with PBS-T, the TMB substrate (3,3,5,5 tetramethylbenzidine; Sigma, St Louis, MO) was used for detecting peroxidase activity before addition of 1M H_2SO_4 to stop the reaction. Absorbance was measured at 450 nm.

MTS cell viability assay

Five thousand cancer cells were dispensed in each well of sterile 96-well flat-bottom plates the day before starvation in RPMI complete medium/1% FCS for 18h. Ten-fold dilutions of

anti-HER3 antibodies were then added for 5 days, with or without $3x10^{-9}$ M NRG1-β1 ECD. Cell viability was then measured using the CellTiter 96 Aqueous One Solution Cell Proliferation Assay (Promega, Madison, WI). Colorimetry was measured at 490 nm absorbance. All experiments were done in triplicate.

ADCC assay

Twenty thousand MDA-MB-453 breast carcinoma cells (target; T) were added to each well of sterile flat-bottom 96-well plates. One day later, ten-fold serial dilutions of anti-HER3 antibodies and control Px antibody were added, with or without $3x10^{-9}$ M NRG1-β1 ECD, 30min before addition of peripheral blood mononuclear cells (PBMCs) as effector cells (E). PBMCs from healthy donors (Etablissement Français du Sang) were prepared by density gradient centrifugation (GE Healthcare) according to the manufacturer's instructions, and 300,000 cells were added to each well (15:1 E:T ratio). ADCC was assessed using the Cytotox 96 Non-radioactive Cytotoxicity Assay (Promega) that measures the release of lactate dehydrogenase (LDH) from damaged cells. After 20h of incubation, measurement was performed according to the manufacturer's instructions. The percentage of specific lysis of each sample was determined using the following formula: percentage specific lysis = (sample LDH release – E cell spontaneous LDH release – T cell spontaneous LDH release)/(T cell maximum LDH release – T cell spontaneous LDH release)*100.

HER3/AKT signaling analysis by western blotting

$2x10^{6}$ BxPC3 cells were grown in 10-cm culture plates at 37°C for 24h. After serum starvation in RPMI/1% FCS for 18h and washing, cells were pre-stimulated with various concentrations of NRG1-β1 ECD ($3x10^{-12}$ M to $3x10^{-9}$ M) for 5min, before incubation with 330nM of anti-HER3 antibodies at 37°C for 25min. Alternatively, BxPC3 cells, pre-stimulated with $1x10^{-9}$ M NRG1-β1 ECD for 5min, were incubated with ten-fold serial dilutions (from 330 to 0.33nM) of anti-HER3 antibodies for 25min. Cells were then washed, scraped and lysed

with buffer containing 20mM Tris-HCl pH 7.5, 150mM NaCl, 1.5mM $MgCl_2$, 1mM EDTA, 1% Triton, 10% glycerol, 0.1mM phenylmethylsulfonyl fluoride, 100mM sodium fluoride, 1mM sodium orthovanadate (Sigma), and one tablet of complete protease inhibitor mixture (Roche Diagnostics, Indianapolis, IN). After 30min, the insoluble fraction was cleared by centrifugation and protein concentration in cell lysates was determined with the Bradford assay. After SDS-PAGE electrophoresis under reducing conditions, proteins were transferred to polyvinylidene difluoride membranes (Millipore) that were then saturated in TNT buffer (25mM Tris pH 7.4, 150mM NaCl, 0.1% Tween) containing 5% nonfat dry milk at 25°C for 1h. Membranes were incubated with primary antibodies against HER3 or AKT and their phosphorylated forms, diluted in TNT/5% BSA buffer, at 4°C for 18h. After five washes in TNT buffer, the appropriate peroxidase-conjugated secondary antibodies (Sigma) were added in TNT buffer/5% nonfat dry milk at 25°C for 1h. After five washes in TNT buffer, blots were visualized using a chemiluminescent substrate (Western lightning Plus-ECL, Perkin Elmer, Waltham, MA). Positive bands were pixel-quantified using the Image J software and 100% phosphorylation was quantified in NRG1-stimulated cells without antibody.

Phosphorylated AKT and ERK quantification by TR-FRET

Phosphorylated AKT (pAKT) and ERK1/2 (pERK1/2) levels were quantified using the HTRF pAKT Ser473 and pERK Thr202/Tyr204 Kits (Cisbio Bioassay). $5x10^4$ BxPC3 cells/well were seeded in sterile 96-well flat-bottom plates and cultured overnight before starvation in RPMI/1% FCS for 18h. After removing the medium, cells were pre-stimulated with low ($1x10^{-9}$ M) or high ($1x10^{-7}$ M) concentrations of NRG1-β1 ECD for 5min, before adding ten-fold or two-fold dilutions of anti-HER3 antibodies, starting from 330nM, for another 25min at 37°C. NRG1 and the antibodies were removed by extensive washing and cells were lysed in the supplemented lysis buffer (Cisbio Bioassay). Plates were incubated at room temperature with shaking for 30min to lyse cells. Lysates were transferred to white 384-well plates. Anti-pERK1/2-cryptate/anti-pERK1/2-d2 or anti-pAKT-cryptate/anti-pAKT-d2 antibody pairs were added to each well and left in the dark at room temperature for 4h. The TR-FRET signal (665

nm/620 nm emission ratio) was measured on a Pherastar FS reader and normalized to 100% binding. Negative control wells contained unstimulated/non-treated cells and labeled antibodies, whereas 100% binding was obtained by stimulating BxPC3 cells with NRG1 without antibody treatment. Experiments were done in triplicate.

Quantitative PCR analysis

Total RNA was isolated from HCC-1806, BxPC3, HPAC and A549 cells using the RNeasy® Mini Kit (Zymo Research, Irvine, CA). RNA was quantified by UV spectroscopy. Total RNA (1µg) was reverse-transcribed using the M-MLV Kit (Invitrogen). Real-time quantitative PCR was performed using a LightCycler® 480 instrument (Roche Diagnostics), according to the manufacturer's instructions. The amplification specificity was checked by melting curve analysis. Real-time PCR values were determined by reference to a standard curve that was generated by real-time PCR amplification of a serially diluted cDNA sample using primers specific for *NRG1α, NRG1β, EGF* and Hypoxanthine Phosphoribosyl Transferase (*HPRT*). Data were normalized to the reference gene *HPRT*.

Tumor xenografts and treatment

All *in vivo* experiments were performed in compliance with the French regulations and ethical guidelines for experimental animal studies in an accredited establishment (Agreement No. C34-172-27). BxPC3 ($3x10^6$), HCC-1806 ($1x10^6$), A549 ($4x10^6$) and HPAC ($3.5x10^6$) cancer cells were subcutaneously injected in the right flank of six-week-old female athymic mice (Harlan; Indianapolis, IN). Tumor-bearing mice were randomized to different treatment groups (at least six animals/group) when tumors reached a volume of 100 mm^3. Animals were treated by intraperitoneal injection of 15mg/kg of ch9F7-F11-Emb or H4B-121-Emb twice a week for 4 weeks. Tumor volumes were calculated by using the formula: $D_1 \times D_2 \times D_3 /2$. For survival analysis, mice were sacrificed when tumors reached a volume of 1500 or 2000 mm^3.

Results

NRG1 is a positive allosteric modulator of 9F7-F11 binding to HER3

We previously showed that 9F7-F11 does not compete with NRG1 for binding to HER3 in SKBR3 cells (43). Now we tested whether NRG1 influenced the binding of 9F7-F11 or of other antibodies to HER3 using a cell-based HTRF assay. First, we confirmed by ELISA that ch9F7-F11-Emb and H4B-121-Emb, U3-1287, Ab#6, Mab205.10.2 and MOR09825 bound equally to HER3 in a dose-dependent manner, with similar half-maximal concentrations (EC_{50}; from 0.11 to 0.44nM) (Fig.1A). However, the HTRF assay showed that binding of d2-labeled H4B-121-Emb, U3-1287, Ab#6, Mab205.10.2 and MOR09825 to HER3 in SNAP-Tag lumi4-Tb HER3-expressing HEK293 cells was abrogated in a dose-dependent manner upon co-incubation with increasing concentrations of NRG1. Only binding of d2-labeled ch9F7-F11-Emb to HER3 was increased by 13-fold upon co-incubation with NRG1 (Fig.1B). Similarly, binding of 9F7-F11 to HER3 was enhanced 15-fold by co-incubation with NRG1, while binding of H4B-121 was completely abolished (Supplementary Fig.S1). As a positive control, binding of d2-labeled NRG1 to HER3 was inhibited by free NRG1 (Fig.S1). These results suggest that 9F7-F11, differently from other anti-HER3 antibodies, binds to a unique allosteric epitope outside the NRG1 binding site, and demonstrate that NRG1 is a positive allosteric modulator of 9F7-F11 binding to HER3.

Reciprocally, binding of d2-labeled NRG1 to SNAP-Tag lumi4-Tb HER3-expressing HEK293 cells was inhibited by co-incubation of all the anti-HER3 antibodies tested, except ch9F7-F11-Emb (Fig.1C) and 9F7-F11 (Fig.S2) that increased by 1.5-fold NRG1 binding to HER3. The control antibody Px did not affect NRG1 binding to HER3 (Fig.1C). Taken together, these results indicate that NRG1 improves 9F7-F11 binding to HER3, whereas it inhibits binding of ligand-competing anti-HER3 antibodies.

9F7-F11 inhibits cancer cell viability and this effect is enhanced by NRG1

Co-incubation with 3nM NRG1 enhanced the dose-dependent inhibitory effect of 9F7-F11 (non-ligand competing anti-HER3 antibody) on BxPC3 and HPAC pancreatic cell viability compared with control cells (no NRG1), whereas no improvement was observed for the H4B-121 antibody. The control antibody Px, did not have any effect on cell viability both with or without NRG1 (Fig. 2).

NRG1 enhances 9F7-F11-mediated ADCC and reduces H4B-121-mediated ADCC

ADCC is one of the main mechanisms of action of therapeutic antibodies and is increased when using antibodies with low-fucose Fc. Accordingly, low-fucose ch9F7-F11-Emb and H4B-121-Emb showed a stronger dose-dependent binding to the CD16a receptor (FcγRIIIA) by ELISA than ch9F7-F11 and H4B-121 (Fig.3A). This translated into higher and dose-dependent ADCC of MDA-MB-453 breast cancer cells by PBMCs in the presence of ch9F7-F11-Emb and H4B-121-Emb than with ch9F7-F11 and H4B-121 (Fig.3B; upper panel). The control antibody Px did not induce ADCC. Addition of 3nM NRG1 intensified ADCC mediated by native or low-fucose ch9F7-F11 (Fig.3B; compare lower and upper panels). Conversely, NRG1 almost fully inhibited ADCC induced by H4B-121 and dramatically reduced ADCC mediated by H4B-121-Emb (Fig.3B).

9F7-F11 is a negative allosteric modulator of NRG1-mediated cell signaling

Most anti-HER3 antibodies hinder HER3-triggered cell signaling in cancer cells, mainly by blocking the PI3K/AKT and ERK pathways. Therefore, the effect of 330nM ch9F7-F11-Emb or H4B-121-Emb in BxPC3 pancreatic cancer cells pre-incubated with increasing concentrations of NRG1 (from $3x10^{-12}$ to $3x10^{-9}$ M) was evaluated by western blotting. NRG1 induced, in a dose-dependent manner, HER3 phosphorylation at Tyr1289, Tyr1197 and Tyr1222 (p85-binding sites), and consequently AKT phosphorylation on Ser473 (Fig.4). The maximal phosphorylation was observed with 1nM NRG1. ch9F7-F11-Emb completely abrogated ligand-mediated HER3 and AKT phosphorylation, independently of the NRG1

concentration. Conversely, H4B-121-Emb partially reduced HER3 and AKT phosphorylation induced by low (0.003 to 0.03nM), but not high (1-3nM) NRG1 concentrations. Similarly, HER3 (Tyr1289, Tyr1197 and Tyr1222) and AKT (Ser473) phosphorylation induced by pre-stimulation with 1nM NRG1 were inhibited, in a dose-dependent manner, by incubation with increasing (0.33-330nM) concentrations of ch9F7-F11-Emb in BxPC3 cells (EC_{50}: 3.3nM of antibody) (Fig.S3). In the same conditions, H4B-121-Emb did not affect phosphorylation of HER3 on Tyr1289 and of AKT on Ser476 (Fig.S3). Taken together, these results again suggest that 9F7-F11 is a negative-allosteric modulator of NRG1-mediated cell signaling and that it is more efficient than the NRG1-competing antibody H4B-121. Moreover, 9F7-F11, but not H4B-121, effect on cell signaling was independent of NRG1 concentration.

Then, TR-FRET was used to quantify and compare the effect of ch9F7-F11-Emb and of other anti-HER3 antibodies (U3-1287, Ab#6, Mab205.10.2 and MOR09825) on ligand-induced cell signaling. Like H4B-121-Emb, these antibodies block NRG1 binding, except MOR09825 (47). TR-FRET analysis confirmed that ch9F7-F11-Emb strongly reduced NRG1-induced AKT phosphorylation on Ser473, independently of NRG1 concentration (1nM or 100nM), with an EC_{50} of about 0.33nM (Fig.5A). This was confirmed using 9F7-F11 or ch9F7-F11 (Fig.S4). All the other anti-HER3 antibodies also inhibited AKT phosphorylation (EC_{50} between 33 and 330nM) after stimulation with 1nM NRG1, although less efficiently than ch9F7-F11-Emb. Moreover, their inhibitory effect was completely abrogated, except for MOR09825, when cells were pre-stimulated with 100nM NRG1. Similarly, NRG1-mediated ERK1/2 phosphorylation on Thr202/Tyr204 was most efficiently inhibited by ch9F7-F11-Emb (EC_{50} of about 33nM compared with EC_{50} up to 330nM for the other antibodies). Such inhibition was blocked when cells were pre-stimulated with 100nM NRG1, except when using ch9F7-F11-Emb and MOR09825 (Fig.5B). The TR-FRET results on the antibody-mediated inhibition of NRG1-induced cell signaling confirm those obtained by western blotting, and strengthen the unique pharmacological profile of ch9F7-F11-Emb as a negative-allosteric modulator of NRG1 activity, independently of the ligand concentration.

The non-ligand competing 9F7-F11 reduces tumor growth of NRG1-positive tumors more efficiently than the ligand-competing H4B-121 antibody

We finally asked whether 9F7-F11 profile (negative-allosteric modulator of NRG1 activity favored by ligand permeation) could translate into a better anti-tumor efficacy *in vivo*. Athymic mice were xenografted with NRG1-expressing tumor cells (pancreatic BxPC3, lung A549 and TNBC HCC-1806) or with NRG1-negative HPAC pancreatic tumor cells. *NRG1*α, *NRG1*β and *EGF* mRNA expression in these cells were quantified by qPCR analysis (Fig.S5). NRG1 did not affect *in vitro* cell proliferation of HCC-1806, A549 and HPAC cells, but increased viability of BxPC3 cells (Fig.S6). ch9F7-F11-Emb treatment reduced growth of NRG1-expressing BxPC3, HCC-1806 and A549 tumor cell xenografts more potently than H4B-121-Emb (Fig.6A-C, left panels). Interestingly, this effect was observed in cancer cells that express HER3 at very low level (*e.g.,* A549 cells) and translated into a longer survival (Fig.6A-C, right panels). Specifically, the mean tumor growth inhibition in ch9F7-F11-Emb and H4-B121-Emb treated mice was 95% *vs* 75% at day 49 post-BxPC3 cell graft, 70% *vs* 48% at day 36 post-HCC-1806 cell graft, and 75% *vs* 20% at day 72 post-A549 cell graft, respectively. In contrast, in mice bearing NRG1-negative HPAC tumor cell xenografts, treatment with ch9F7-F11-Emb or H4-B121-Emb led to the same mean tumor growth inhibition (40%) at day 40 post-graft (Fig. 6D, left panel) and to a similar survival rate (Fig.6D, right panel). Altogether, these *in vivo* results demonstrate that the non-NRG1 competing allosteric modulator 9F7-F11 inhibits tumor growth of NRG1-positive pancreatic, lung and breast cancers more efficiently than the NRG1-competing orthosteric H4B-121 antibody, in agreement with the effects observed *in vitro* on NRG1-mediated cell viability, signaling and ADCC.

Discussion

Here, we show that the dual-allosteric modulator 9F7-F11 is well designed for the treatment of NRG1-positive tumors because stimulation with high NRG1 concentrations promotes its binding to HER3 and its biological effects in cancer cells. 9F7-F11 unique pharmacological profile has never been observed in all the previously described anti-HER3 antibodies that mostly act by blocking NRG1 binding and the binding of which is reciprocally inhibited by NRG1 (40). The non-ligand competing 9F7-F11 antibody profile is better fitted for targeting NRG1-positive tumors than the U3-1287, Ab#6 and Mab205.10.2 antibodies that directly block ligand binding (26,46,48), or the MOR09825 or KTN3379 antibodies that preferentially bind to HER3 in the inactive configuration (47,49). Indeed, in NRG1-positive tumors, the ligand might be already bound to HER3 before antibody treatment, leading *in vivo* to a prevalence of HER3 receptors in the active conformation. Moreover, in HER2-amplified tumors, where HER3-HER2 heterodimers can be formed independently of NRG1 activation, HER3 targeted therapy is less effective, as confirmed recently in a phase II clinical trial in ovarian cancer (2). 9F7-F11 shows a unique HER3 binding profile because it is promoted by NRG1 presence. Garner et al. (47) showed that the anti-HER3 antibody LJM716 targets a conformational epitope located within domains 2 and 4 of HER3 inactive configuration and does not prevent NRG1 binding to HER3. Such binding characteristics have been demonstrated using pre-formed HER3/LJM716 complexes to avoid subsequent binding of various concentrations of NRG1 to the receptor (47). In our co-incubation experiments (Fig.1C), less than 1nM of free MOR09825 (the parental antibody of LJM716) could displace 50% of the binding of 20nM d2-conjugated NRG1 to lumi4-Tb-HER3-expressing HEK293 cells. Reciprocally, higher NRG1 concentrations (around 100nM) were necessary to efficiently shift the equilibrium of 0.5nM MOR09825 complexed with HER3 towards the extended active conformation (Fig.1B). Thus, in our experimental conditions, MOR09825 acts as a ligand-blocking antibody with a slow off-rate and its HER3 binding affinity is greater than that of NRG1. We can speculate that the high-affinity barrier imposed by pre-formed

LJM716/HER3 complexes cannot be overcome by subsequent addition of NRG1 that shows lower affinity to HER3 compared with the antibody. In contrast, when 1 or 100nM NRG1 is added before antibody treatment, only the highest MOR09825 concentration could displace the ligand from HER3 and inhibit ligand-mediated AKT and ERK1/2 phosphorylation. In this case, 9F7-F11 was more efficient than MOR09825 at inhibiting signaling, independently of the ligand concentration. The other ligand-competitive antibodies (U3-1287, Ab#6, Mab205.10.2 and H4B-121) did not work at high NRG1 concentration.

Nevertheless, the definition of “physiological” NRG1 concentration within tumors (as opposed to NRG1 addiction) is still an unresolved issue. An NRG1 detection/quantification assay could be of great value for selecting patients who could benefit of anti-HER3 treatment. NRG1 expression in head and neck, esophageal, lung and cervical cancers could be higher than in other tumor types (4,10,13,50); moreover, acquired NRG1 expression could also drive resistance to targeted therapies (5,25,28). Normal NRG1 plasma level (28,51–54) and NRG1 concentration in body fluids in various diseases (51,52,54–56), including colorectal (57), lung (7,25,28,58) and ovarian (58) cancers, are in the picomolar-nanomolar range and higher level in cancers are considered to be a predictive biomarker for HER3 targeted therapy (5). Currently, there is no standard measurement to define NRG1 level (low or high) in tumors *in situ*. MacBeath et al. (3) defines high NRG1 as >5 by RT-qPCR or ≥1+ by RNA-in situ hybridization. We can postulate that NRG1 concentration within tumors is higher than in body fluids and becomes an obstacle for the efficiency of ligand-blocking anti-HER3 antibodies. This could explain the disappointing results of phase III clinical trials on NRG1-competitive HER3 antibodies (NCT02134015). Therefore, NRG1 should be quantified in tumor tissue biopsies just before treatment decision-making. The optimal method of detection (RNA-in situ hybridization or RT-PCR), threshold for NRG1 positivity (continuous variable) and the reliability of results obtained with primary archived tissues compared with fresh tumor biopsies are still debated.

Moreover, we think that besides NRG1-overexpressing tumors, 9F7-F11 could be effective also in other cancer subtypes that harbor NRG1 fusion genes (29–33). These fusion genes

lead to NRG1 expression at the tumor cell surface and to NRG1 binding to HER3 in an autocrine or juxtacrine manner. In these tumors, active HER3 receptors are continuously permeated by NRG1 fusion proteins, and 9F7-F11, which binds to ligand-targeted HER3 with greater affinity than to HER3-inactive monomers, could be very efficient. This antibody could also be useful for tumors that are activated through paracrine ligand-receptor stimulation from the cell microenvironment (35–39).

Receptors from the HER family are flexible molecules which can be ortho- or allosterically activated, depending on the ligand type and its binding site. HER behavior can closely resemble that of GPCR activation and trans-conformation (41). Therefore, the nature of the allosteric interaction (e.g., 9F7-F11 binding to HER3) could be closely dependent on the orthosteric ligand (the probe), in accordance with the concept of probe-dependence and biased signaling developed for GPCR (42). Here, we demonstrate by TR-FRET analysis that 9F7-F11 binding to HER3 is promoted by the presence of the orthosteric ligand NRG1 and, reciprocally, that 9F7-F11 binding to HER3 increases NRG1 binding. The resulting output is the inhibition of NRG1-mediated signaling and, more largely, the intensification of the *in vitro* and *in vivo* antibody-mediated biological effects when NRG1 permeates tumor cells. This dual-allosteric profile (i.e., positive cooperativity for NRG1 binding and simultaneously negative modulation of NRG1-mediated effects) has been already demonstrated for Org 27569, an allosteric modulator of cannabinoid receptor 1 (59). Tailoring allosteric antibodies against the HER family of receptors by using “oriented” immunization strategies has been already investigated with the anti-EGFR antibody mAb806 (60) that recognizes a conformationally exposed epitope in tumors that overexpress wild type EGFR or mutant EGFRvIII. However, to our knowledge, this is the first report showing that receptor targeting by an antibody (9F7-F11) is increased in the presence of the orthosteric ligand. The mechanism of action of other drugs might bring some clues. Org 27569 stabilizes cannabinoid receptor 1 structure in a conformation at the transmembrane level that is different from the one observed during “classical” GPCR activation (59). The anti-EGFR antibody mAb806 targets an epitope on the D2 extracellular domain that is masked in the

inactive monomer and in ligand-activated dimers, but exposed when EGFR is overexpressed, or upon EGFR extracellular domain truncation (61) or glycosylation changes (62). Interestingly, it has been suggested that HER3 glycosylation changes are crucial for NRG1-induced dimer formation, cell signaling and tumor progression (63,64). The 9F7-F11 antibody binds to an epitope located in the D1 domain of HER3 (43). Despite the different binding profile, 9F7-F11 specificity also suggests a conformation-sensitive epitope that is partially masked in the inactive monomer and better exposed in the NRG1-liganded HER3. Finally, NRG1 activates HER3, but also HER4, to transduce efficient signaling, mainly through the AKT and ERK pathways. It has been shown that the NRG1/HER4-inducible Hippo pathway promotes YAP-driven oncogenic mechanisms through the binding of the PPxY motif in HER4 to the WW domains of YAP (65). HER3 also harbors a PPxY domain that could be involved in 9F7-F11-induced HER3 degradation (45). Thus, HER3 may act as an alternative activator of the Hippo-YAP pathway that could, therefore, be indirectly blocked by the anti-HER3 antibody 9F7-F11.

In summary, we demonstrated that the binding to HER3 and biological effects on tumor cells of the novel, very potent dual-allosteric anti-HER3 antibody 9F7-F11 are paradoxically facilitated by the natural ligand NRG1. Therefore, by hijacking NRG1 addiction of cancer cells to promote its inhibitory effects on NRG1-mediated tumor growth and resistance, 9F7-F11 displays a unique potential for targeted treatment of NRG1-positive cancers.

Acknowledgements

We thank G. Heintz and S. Bousquié (IRCM) for cell culture and antibody production. The animal facility staff at the IRCM is greatly acknowledged. We also thank S. Kadi (Cisbio) for performing antibody labeling and TagLite assays.

References

1. Juric D, Dienstmann R, Cervantes A, Hidalgo M, Messersmith W, Blumenschein GR, et al. Safety and Pharmacokinetics/Pharmacodynamics of the First-in-Class Dual Action HER3/EGFR Antibody MEHD7945A in Locally Advanced or Metastatic Epithelial Tumors. Clin Cancer Res Off J Am Assoc Cancer Res. 2015;21:2462–70.

2. Liu JF, Ray-Coquard I, Selle F, Poveda AM, Cibula D, Hirte H, et al. Randomized Phase II Trial of Seribantumab in Combination With Paclitaxel in Patients With Advanced Platinum-Resistant or -Refractory Ovarian Cancer. J Clin Oncol. 2016;JCO.2016.67.1891.

3. Macbeath, G., Adiwijaya, B., Liu, J., Sequist, L.V., Pujade-Lauraine, E., Higgins, M., et al. A meta-analysis of biomarkers in three randomized, phase 2 studies of MM-121, a ligand-blocking anti-ERBB3 antibody, in patients with ovarian, lung, and breast cancers. Ann Oncol. 2014;25:iv58-iv84.

4. Mathews, S., Finn, G., Kudla, A.J., Rimkunas, V., Laivins, P., Macbeath, G., et al. Identification of Heregulin (HRG) expression as a driver of a difficult-to-treat cancer phenotype and development of a companion diagnostic for the HRG-ErbB3 targeting drug seribantumab. AACR Precis Med Ser. 2016;Abstract A19:Miami.

5. Mendell J, Freeman DJ, Feng W, Hettmann T, Schneider M, Blum S, et al. Clinical Translation and Validation of a Predictive Biomarker for Patritumab, an Anti-human Epidermal Growth Factor Receptor 3 (HER3) Monoclonal Antibody, in Patients With Advanced Non-small Cell Lung Cancer. EBioMedicine. 2015;2:264–71.

6. Meulendijks D, Jacob W, Martinez-Garcia M, Taus A, Lolkema MP, Voest EE, et al. First-in-Human Phase I Study of Lumretuzumab, a Glycoengineered Humanized Anti-HER3 Monoclonal Antibody, in Patients with Metastatic or Advanced HER3-Positive Solid Tumors. Clin Cancer Res Off J Am Assoc Cancer Res. 2016;22:877–85.

7. Yonesaka K, Hirotani K, Von Pawel J, Dediu M, Chen S, Copigneaux C, et al. Soluble heregulin, HER3 ligand, to predict the efficacy of anti-HER3 antibody patritumab combination with erlotinib in randomized phase II study, HERALD, for non-small cell lung cancer. ASCO Meet Abstr. 2016;34:9071.

8. Meetze K, Vincent S, Tyler S, Mazsa EK, Delpero AR, Bottega S, et al. Neuregulin 1 expression is a predictive biomarker for response to AV-203, an ERBB3 inhibitory antibody, in human tumor models. Clin Cancer Res Off J Am Assoc Cancer Res. 2015;21:1106–14.

9. Ocaña A, Díez-González L, Esparís-Ogando A, Montero JC, Amir E, Pandiella A. Neuregulin expression in solid tumors: Prognostic value and predictive role to anti-HER3 therapies. Oncotarget. 2016;

10. Shames DS, Carbon J, Walter K, Jubb AM, Kozlowski C, Januario T, et al. High heregulin expression is associated with activated HER3 and may define an actionable biomarker in patients with squamous cell carcinomas of the head and neck. PloS One. 2013;8:e56765.

11. Ocana A, Vera-Badillo F, Seruga B, Templeton A, Pandiella A, Amir E. HER3 overexpression and survival in solid tumors: a meta-analysis. J Natl Cancer Inst. 2013;105:266–73.

12. Montero JC, Rodríguez-Barrueco R, Ocaña A, Díaz-Rodríguez E, Esparís-Ogando A, Pandiella A. Neuregulins and cancer. Clin Cancer Res Off J Am Assoc Cancer Res. 2008;14:3237–41.

13. Wilson TR, Lee DY, Berry L, Shames DS, Settleman J. Neuregulin-1-mediated autocrine signaling underlies sensitivity to HER2 kinase inhibitors in a subset of human cancers. Cancer Cell. 2011;20:158–72.

14. Zhou B-BS, Peyton M, He B, Liu C, Girard L, Caudler E, et al. Targeting ADAM-mediated ligand cleavage to inhibit HER3 and EGFR pathways in non-small cell lung cancer. Cancer Cell. 2006;10:39–50.

15. Li Q, Ahmed S, Loeb JA. Development of an autocrine neuregulin signaling loop with malignant transformation of human breast epithelial cells. Cancer Res. 2004;64:7078–85.

16. Schaefer G, Fitzpatrick VD, Sliwkowski MX. Gamma-heregulin: a novel heregulin isoform that is an autocrine growth factor for the human breast cancer cell line, MDA-MB-175. Oncogene. 1997;15:1385–94.

17. Yuste L, Montero JC, Esparís-Ogando A, Pandiella A. Activation of ErbB2 by overexpression or by transmembrane neuregulin results in differential signaling and sensitivity to herceptin. Cancer Res. 2005;65:6801–10.

18. Gollamudi M, Nethery D, Liu J, Kern JA. Autocrine activation of ErbB2/ErbB3 receptor complex by NRG-1 in non-small cell lung cancer cell lines. Lung Cancer Amst Neth. 2004;43:135–43.

19. al Moustafa AE, Alaoui-Jamali M, Paterson J, O'Connor-McCourt M. Expression of P185erbB-2, P160erbB-3, P180erbB-4, and heregulin alpha in human normal bronchial epithelial and lung cancer cell lines. Anticancer Res. 1999;19:481–6.

20. Sheng Q, Liu X, Fleming E, Yuan K, Piao H, Chen J, et al. An activated ErbB3/NRG1 autocrine loop supports in vivo proliferation in ovarian cancer cells. Cancer Cell. 2010;17:298–310.

21. Phillips GDL, Fields CT, Li G, Dowbenko D, Schaefer G, Miller K, et al. Dual targeting of HER2-positive cancer with trastuzumab emtansine and pertuzumab: critical role for neuregulin blockade in antitumor response to combination therapy. Clin Cancer Res Off J Am Assoc Cancer Res. 2014;20:456–68.

22. Xia W, Petricoin EF, Zhao S, Liu L, Osada T, Cheng Q, et al. An heregulin-EGFR-HER3 autocrine signaling axis can mediate acquired lapatinib resistance in HER2+ breast cancer models. Breast Cancer Res BCR. 2013;15:R85.

23. Curley MD, Sabnis GJ, Wille L, Adiwijaya BS, Garcia G, Moyo V, et al. Seribantumab, an Anti-ERBB3 Antibody, Delays the Onset of Resistance and Restores Sensitivity to Letrozole in an Estrogen Receptor-Positive Breast Cancer Model. Mol Cancer Ther. 2015;14:2642–52.

24. Kawakami H, Okamoto I, Yonesaka K, Okamoto K, Shibata K, Shinkai Y, et al. The anti-HER3 antibody patritumab abrogates cetuximab resistance mediated by heregulin in colorectal cancer cells. Oncotarget. 2014;5:11847–56.

25. Yonesaka K, Zejnullahu K, Okamoto I, Satoh T, Cappuzzo F, Souglakos J, et al. Activation of ERBB2 signaling causes resistance to the EGFR-directed therapeutic antibody cetuximab. Sci Transl Med. 2011;3:99ra86.

26. Garrett JT, Sutton CR, Kuba MG, Cook RS, Arteaga CL. Dual blockade of HER2 in HER2-overexpressing tumor cells does not completely eliminate HER3 function. Clin Cancer Res Off J Am Assoc Cancer Res. 2013;19:610–9.

27. Iida M, Brand TM, Starr MM, Huppert EJ, Luthar N, Bahrar H, et al. Overcoming acquired resistance to cetuximab by dual targeting HER family receptors with antibody-based therapy. Mol Cancer. 2014;13:242.

28. Yonesaka K, Kudo K, Nishida S, Takahama T, Iwasa T, Yoshida T, et al. The pan-HER family tyrosine kinase inhibitor afatinib overcomes HER3 ligand heregulin-mediated resistance to EGFR inhibitors in non-small cell lung cancer. Oncotarget. 2015;6:33602–11.

29. Dhanasekaran SM, Balbin OA, Chen G, Nadal E, Kalyana-Sundaram S, Pan J, et al. Transcriptome meta-analysis of lung cancer reveals recurrent aberrations in NRG1 and Hippo pathway genes. Nat Commun. 2014;5:5893.

30. Fernandez-Cuesta L, Plenker D, Osada H, Sun R, Menon R, Leenders F, et al. CD74-NRG1 fusions in lung adenocarcinoma. Cancer Discov. 2014;4:415–22.

31. Murayama T, Nakaoku T, Enari M, Nishimura T, Tominaga K, Nakata A, et al. Oncogenic Fusion Gene CD74-NRG1 Confers Cancer Stem Cell-like Properties in Lung Cancer through a IGF2 Autocrine/Paracrine Circuit. Cancer Res. 2016;76:974–83.

32. Nakaoku T, Tsuta K, Ichikawa H, Shiraishi K, Sakamoto H, Enari M, et al. Druggable oncogene fusions in invasive mucinous lung adenocarcinoma. Clin Cancer Res Off J Am Assoc Cancer Res. 2014;20:3087–93.

33. Wang XZ, Jolicoeur EM, Conte N, Chaffanet M, Zhang Y, Mozziconacci MJ, et al. gamma-heregulin is the product of a chromosomal translocation fusing the DOC4 and HGL/NRG1 genes in the MDA-MB-175 breast cancer cell line. Oncogene. 1999;18:5718–21.

34. Fernandez-Cuesta L, Thomas RK. Molecular Pathways: Targeting NRG1 Fusions in Lung Cancer. Clin Cancer Res Off J Am Assoc Cancer Res. 2015;21:1989–94.

35. Capparelli C, Rosenbaum S, Berger AC, Aplin AE. Fibroblast-derived neuregulin 1 promotes compensatory ErbB3 receptor signaling in mutant BRAF melanoma. J Biol Chem. 2015;290:24267–77.

36. Cheng H, Terai M, Kageyama K, Ozaki S, McCue PA, Sato T, et al. Paracrine Effect of NRG1 and HGF Drives Resistance to MEK Inhibitors in Metastatic Uveal Melanoma. Cancer Res. 2015;75:2737–48.

37. De Boeck A, Pauwels P, Hensen K, Rummens J-L, Westbroek W, Hendrix A, et al. Bone marrow-derived mesenchymal stem cells promote colorectal cancer progression through paracrine neuregulin 1/HER3 signalling. Gut. 2013;62:550–60.

38. Sato Y, Yashiro M, Takakura N. Heregulin induces resistance to lapatinib-mediated growth inhibition of HER2-amplified cancer cells. Cancer Sci. 2013;104:1618–25.

39. Liles JS, Arnoletti JP, Kossenkov AV, Mikhaylina A, Frost AR, Kulesza P, et al. Targeting ErbB3-mediated stromal-epithelial interactions in pancreatic ductal adenocarcinoma. Br J Cancer. 2011;105:523–33.

40. Gaborit N, Lindzen M, Yarden Y. Emerging anti-cancer antibodies and combination therapies targeting HER3/ERBB3. Hum Vaccines Immunother. 2016;12:576–92.

41. Christopoulos A, Changeux J-P, Catterall WA, Fabbro D, Burris TP, Cidlowski JA, et al. International Union of Basic and Clinical Pharmacology. XC. multisite pharmacology: recommendations for the nomenclature of receptor allosterism and allosteric ligands. Pharmacol Rev. 2014;66:918–47.

42. Wootten D, Christopoulos A, Sexton PM. Emerging paradigms in GPCR allostery: implications for drug discovery. Nat Rev Drug Discov. 2013;12:630–44.

43. Lazrek Y, Dubreuil O, Garambois V, Gaborit N, Larbouret C, Le Clorennec C, et al. Anti-HER3 domain 1 and 3 antibodies reduce tumor growth by hindering HER2/HER3 dimerization and AKT-induced MDM2, XIAP, and FoxO1 phosphorylation. Neoplasia N Y N. 2013;15:335–47.

44. Thomas G, Chardès T, Gaborit N, Mollevi C, Leconet W, Robert B, et al. HER3 as biomarker and therapeutic target in pancreatic cancer: new insights in pertuzumab therapy in preclinical models. Oncotarget. 2014;5:7138–48.

45. Le Clorennec C, Lazrek Y, Dubreuil O, Larbouret C, Poul M-A, Mondon P, et al. The anti-HER3 (ErbB3) therapeutic antibody 9F7-F11 induces HER3 ubiquitination and degradation in tumors through JNK1/2- dependent ITCH/AIP4 activation. Oncotarget. 2016;

46. Schoeberl B, Pace EA, Fitzgerald JB, Harms BD, Xu L, Nie L, et al. Therapeutically targeting ErbB3: a key node in ligand-induced activation of the ErbB receptor-PI3K axis. Sci Signal. 2009;2:ra31.

47. Garner AP, Bialucha CU, Sprague ER, Garrett JT, Sheng Q, Li S, et al. An antibody that locks HER3 in the inactive conformation inhibits tumor growth driven by HER2 or neuregulin. Cancer Res. 2013;73:6024–35.

48. Mirschberger C, Schiller CB, Schräml M, Dimoudis N, Friess T, Gerdes CA, et al. RG7116, a therapeutic antibody that binds the inactive HER3 receptor and is optimized for immune effector activation. Cancer Res. 2013;73:5183–94.

49. Lee S, Greenlee EB, Amick JR, Ligon GF, Lillquist JS, Natoli EJ, et al. Inhibition of ErbB3 by a monoclonal antibody that locks the extracellular domain in an inactive configuration. Proc Natl Acad Sci U S A. 2015;112:13225–30.

50. Ligon GF, Lillquist JS, Seibel SB, Wallweber J, Neumeister V, Rimm DL, et al. Combination of neuregulin with EGFR activation signatures predict activity of the anti-ErbB3 antibody KTN3379 in SCCHN. Cancer Res. 2016;76:1196–1196.

51. Dai Y-N, Zhu J-Z, Fang Z-Y, Zhao D-J, Wan X-Y, Zhu H-T, et al. A case-control study: Association between serum neuregulin 4 level and non-alcoholic fatty liver disease. Metabolism. 2015;64:1667–73.

52. Hama Y, Yabe I, Wakabayashi K, Kano T, Hirotani M, Iwakura Y, et al. Level of plasma neuregulin-1 SMDF is reduced in patients with idiopathic Parkinson's disease. Neurosci Lett. 2015;587:17–21.

53. Moondra V, Sarma S, Buxton T, Safa R, Cote G, Storer T, et al. Serum Neuregulin-1beta as a Biomarker of Cardiovascular Fitness. Open Biomark J. 2009;2:1–5.

54. Pankonin MS, Sohi J, Kamholz J, Loeb JA. Differential distribution of neuregulin in human brain and spinal fluid. Brain Res. 2009;1258:1–11.

55. Geisberg CA, Wang G, Safa RN, Smith HM, Anderson B, Peng X-Y, et al. Circulating neuregulin-1β levels vary according to the angiographic severity of coronary artery disease and ischemia. Coron Artery Dis. 2011;22:577–82.

56. Shibuya M, Komi E, Wang R, Kato T, Watanabe Y, Sakai M, et al. Measurement and comparison of serum neuregulin 1 immunoreactivity in control subjects and patients with schizophrenia: an influence of its genetic polymorphism. J Neural Transm Vienna Austria 1996. 2010;117:887–95.

57. Yonesaka K, Takegawa N, Satoh T, Ueda H, Yoshida T, Takeda M, et al. Combined Analysis of Plasma Amphiregulin and Heregulin Predicts Response to Cetuximab in Metastatic Colorectal Cancer. PloS One. 2015;10:e0143132.

58. Carvalho S, Lindzen M, Lauriola M, Shirazi N, Sinha S, Abdul-Hai A, et al. An antibody to amphiregulin, an abundant growth factor in patients' fluids, inhibits ovarian tumors. Oncogene. 2016;35:438–47.

59. Fay JF, Farrens DL. Structural dynamics and energetics underlying allosteric inactivation of the cannabinoid receptor CB1. Proc Natl Acad Sci U S A. 2015;112:8469–74.

60. Gan HK, Burgess AW, Clayton AHA, Scott AM. Targeting of a conformationally exposed, tumor-specific epitope of EGFR as a strategy for cancer therapy. Cancer Res. 2012;72:2924–30.

61. Garrett TPJ, Burgess AW, Gan HK, Luwor RB, Cartwright G, Walker F, et al. Antibodies specifically targeting a locally misfolded region of tumor associated EGFR. Proc Natl Acad Sci U S A. 2009;106:5082–7.

62. Gan HK, Walker F, Burgess AW, Rigopoulos A, Scott AM, Johns TG. The epidermal growth factor receptor (EGFR) tyrosine kinase inhibitor AG1478 increases the formation of inactive untethered EGFR dimers. Implications for combination therapy with monoclonal antibody 806. J Biol Chem. 2007;282:2840–50.

63. Takahashi M, Yokoe S, Asahi M, Lee SH, Li W, Osumi D, et al. N-glycan of ErbB family plays a crucial role in dimer formation and tumor promotion. Biochim Biophys Acta. 2008;1780:520–4.

64. Takahashi M, Hasegawa Y, Ikeda Y, Wada Y, Tajiri M, Ariki S, et al. Suppression of heregulin β signaling by the single N-glycan deletion mutant of soluble ErbB3 protein. J Biol Chem. 2013;288:32910–21.

65. Haskins JW, Nguyen DX, Stern DF. Neuregulin 1-activated ERBB4 interacts with YAP to induce Hippo pathway target genes and promote cell migration. Sci Signal. 2014;7:ra116.

Figure legends

Figure 1. ch9F7-F11-Emb is a non-NRG1 competing antibody and NRG1 enhances its binding to HER3. (A) The low-fucose anti-HER3 antibodies H4B-121-Emb and ch9F7-F11-Emb bind to the HER3 receptor with similar EC_{50} as the other anti-HER3 antibodies. Plates were coated with 50ng/well of recombinant human HER3 ECD at 4°C for 18h and then blocked with 2% BSA in PBS. Anti-HER3 antibodies were serially diluted (from 6.6nM to 0.1nM) and added to the plates at 37°C for 1h. After washes with PBS/0.1% Tween 20, bound anti-HER3 antibodies were detected by incubation with a HRP-$F(ab')_2$ goat anti-human $F(ab')_2$ antibody at 37°C for 2h and then by using TMB as substrate for detecting peroxidase activity at 450nm. **(B)** NRG1 is a positive-allosteric modulator of ch9F7-F11-Emb binding to HER3. Differently from H4B-121-Emb and the other anti-HER3 antibodies, ch9F7-F11-Emb did not compete with the ligand NRG1 and its binding to HER3 increased in the presence of NRG1. SNAP-Tag Lumi4^{TM}-Tb HER3-expressing HEK293 cells were co-incubated with various concentrations of unlabeled NRG1 and 0.5nM d2-conjugated anti-HER3 antibodies. After 5h30 incubation, the time-resolved fluorescence (665 nm/620 nm emission delta ratio) of d2-labeled antibodies bound to HER3 was measured using a Pherastar apparatus and normalized to 100% binding (antibody-d2 conjugates without NRG1, or NRG1-d2 conjugates without antibodies). Results were plotted using the GraphPad Prism software. **(C)** ch9F7-F11-Emb is a positive-allosteric modulator of NRG1 binding to HER3. NRG1 did not compete with ch9F7-F11-Emb for HER3 binding, differently from what observed for the other antibodies, and NRG1 binding to HER3 increased in the presence of ch9F7-F11-Emb. SNAP-Tag Lumi4^{TM}-Tb HER3-expressing HEK293 cells were co-incubated with various concentrations of unlabeled antibodies and 20nM d2-conjugated NRG1. NRG1-d2 binding to HER3 was measured as in (B). For the experiments shown in panels B and C, recombinant human NRG1-β1 ECD and NRG1-β3 EGF domain were used with comparable results.

Figure 2. NRG1 enhances the inhibition of cancer cell viability induced by non-ligand competing 9F7-F11, but not by ligand-competing H4B-121. BxPC3 or HPAC cancer cells were plated in medium with 10% fetal calf serum without NRG1 or in medium with 1% fetal calf serum and 3nM NRG1 and then cultured with increasing concentrations of the indicated antibodies for 5 days. Cell proliferation was measured using the MTS assay. M, medium; Px, irrelevant antibody (control); *P* values for 9F7-F11 vs M (*t* test): *, p<0.05; **, p<0.01; ***, p<0.001.

Figure 3. The low-fucose ch9F7-F11-Emb and H4B-121-Emb antibodies show stronger binding to CD16a (FcγRIIIA) than ch9F7-F11 and H4B-121. (A) The anti-HER3 antibodies H4B121 and ch9F7F11 produced in HEK293 or in YB2/0 cells were mixed with HRP-$F(ab')_2$ goat anti human $F(ab')_2$ antibodies at room temperature for 1h prior to addition to CD16a-coated (200ng per well) ELISA plates at 37°C for 1h. Binding to CD16a was revealed by adding TMB followed by H_2SO_4 to stop the reaction. **(B)** NRG1 enhances ADCC induced by the non-NRG1 competing 9F7-F11 antibody, and reduces ADCC mediated by ligand-competing H4B-121. Target MDA-MB453 breast cancer cells were co-incubated with various concentrations of the anti-HER3 antibodies 9F7-F11, 9F7-F11-Emb, H4B-121 or H4B-121-Emb, without or with 3nM NRG1, and with effector peripheral blood mononuclear cells (T:E ratio 1:15). ADCC was measured by lactate dehydrogenase cell release. The irrelevant Px antibody was used as control (CTRL).

Fig. 4. In pancreatic cancer cells, the non-NRG1 competing allosteric anti-HER3 antibody ch9F7-F11-Emb inhibits NRG1-mediated cell signaling more efficiently than the ligand-competing antibody H4B-121-Emb. BxPC3 cells were pre-stimulated with various concentrations of NRG1 for 5min, before addition of 330nM of antibodies for 25min. After cell lysis, the expression level of total and phosphorylated HER3 (Tyr1289, Tyr1197 and Tyr1222), and total AKT and AKT phosphorylated at Ser473 was measured by western

blotting (**A**) using the appropriate antibodies. HER3 and AKT phosphorylation were then pixel-quantified with Image J (**B)** relative to the maximal phosphorylation (100%) obtained in cells stimulated with NRG1 without antibody treatment ("no Ab"). Results are the mean ± SD of three independent experiments.

Figure 5. High NRG1 level does not affect ch9F7-F11-Emb-mediated inhibition of cell signaling. In pancreatic cancer cells, ch9F7-F11-Emb inhibits in a dose-dependent manner NRG1-induced cell signaling more efficiently than ligand-competing anti-HER3 antibodies. BxPC3 cells were pre-stimulated with 1nM or 100nm NRG1 for 5min, before adding antibodies at various concentrations for another 25min. After cell lysis, the expression levels of AKT phosphorylated at Ser473 and ERK1/2 phosphorylated at Thr202/Tyr204 were quantified by HTRF. The TR-FRET signal (665 nm/620 nm emission ratio) was measured on a Pherastar FS reader relative to the maximal phosphorylation (100%; M) obtained in NRG1-stimulated cells without antibody treatment; *P* values for anti-HER3 antibodies vs M (*t* test): *, $p<0.05$; **, $p<0.01$; ***, $p<0.001$.

Figure 6. The non-NRG1 competing allosteric antibody ch9F7-F11-Emb inhibits tumor growth and increases survival time of mice xenografted with NRG1-positive tumor cells more efficiently than the ligand-competing antibody H4B-121-Emb. Nude mice (n=6/condition) were xenografted with BxPC3 pancreatic cancer cells (**A**), triple-negative breast carcinoma HCC-1806 cells (**B**) or lung A549 cancer cells (**C**) (three NRG1-positive cancer cell lines), or with NRG1-negative pancreatic carcinoma HPAC cells (**D**). When tumors reached a volume of 100 mm^3, mice were treated by intraperitoneal injection of 15 mg/kg of ch9F7-F11-Emb (full black triangles and hatched line), H4B-121-Emb (open grey circles and solid line), or NaCl (full black squares and solid line), twice a week for 4 weeks. Tumor growth data are presented as the mean tumor volume ± S.E.M. for each group of mice. Kaplan-Meier survival curves were calculated when tumors reached a volume of 1500 or 2000 mm^3 and mice were sacrificed. The benefit (gain in days of the treated vs control

group) is indicated on the Kaplan-Meier curves. The gray zone corresponds to the treatment period.

Fig.1

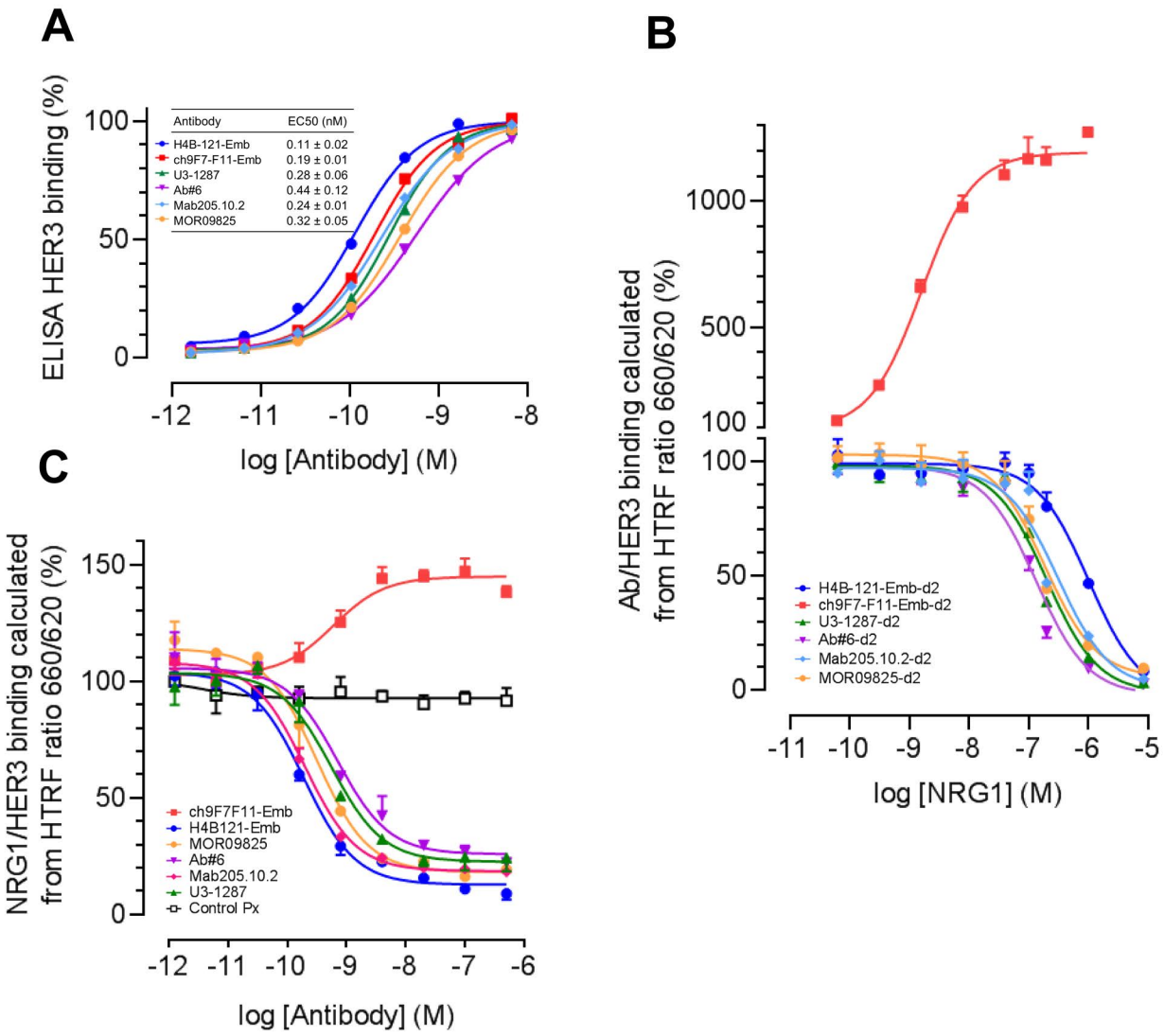
A
ELISA HER3 binding (%)
100
50
0
Antibody
EC50 (nM)
H4B-121-Emb
0.11 ± 0.02
ch9F7-F11-Emb
0.19 ± 0.01
U3-1287
0.28 ± 0.06
Ab#6
0.44 ± 0.12
Mab205.10.2
0.24 ± 0.01
MOR09825
0.32 ± 0.05
-12
-11
-10
-9
-8
log [Antibody] (M)
B
Ab/HER3 binding calculated from HTRF ratio 660/620 (%)
1000
500
100
100
50
0
H4B-121-Emb-d2
ch9F7-F11-Emb-d2
U3-1287-d2
Ab#6-d2
Mab205.10.2-d2
MOR09825-d2
-11
-10
-9
-8
-7
-6
-5
log [NRG1] (M)
C
NRG1/HER3 binding calculated from HTRF ratio 660/620 (%)
150
100
50
0
ch9F7F11-Emb
H4B121-Emb
MOR09825
Ab#6
Mab205.10.2
U3-1287
Control Px
-12
-11
-10
-9
-8
-7
-6
log [Antibody] (M)

Fig.2

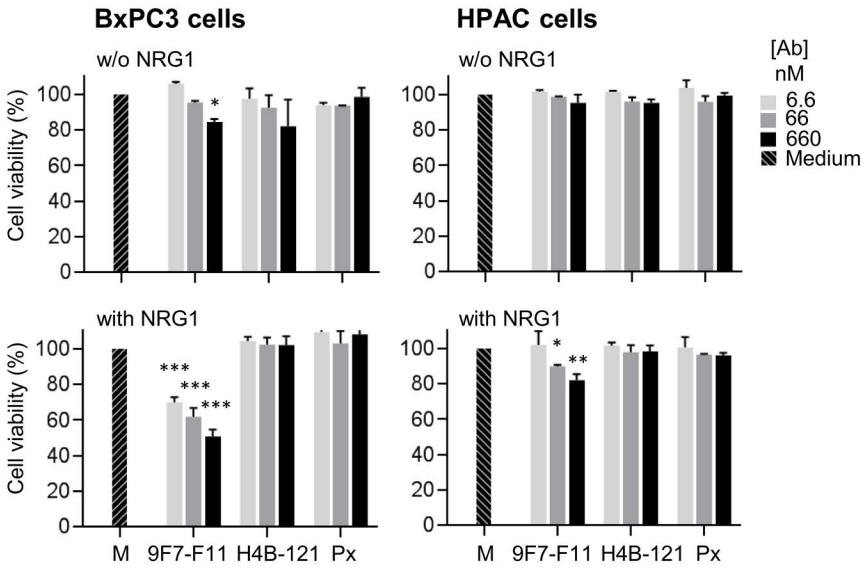
BxPC3 cells
HPAC cells
w/o NRG1
with NRG1
Cell viability (%)
[Ab]
nM
6.6
66
660
Medium
M
9F7-F11
H4B-121
Px

Fig.3

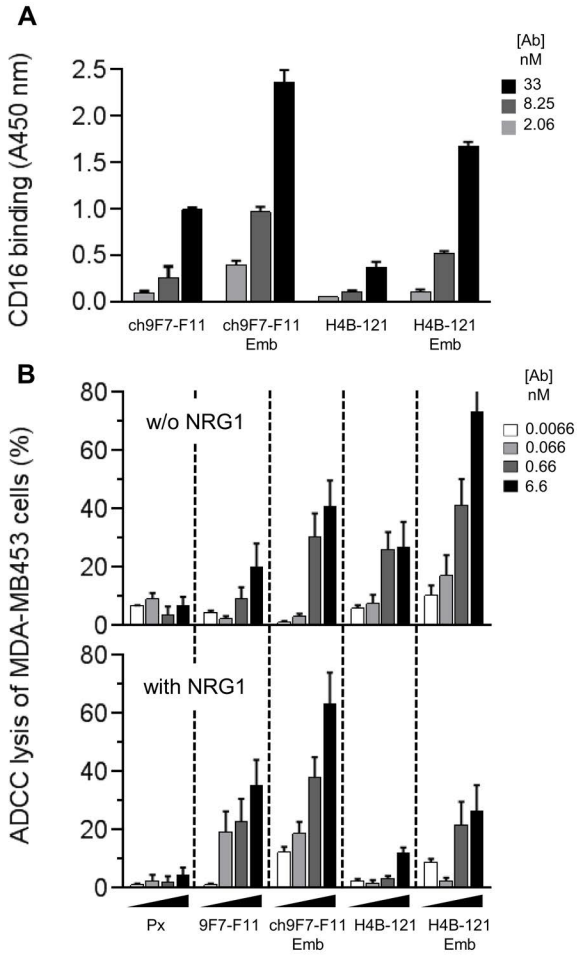
A
CD16 binding (A450 nm)
2.5
2.0
1.5
1.0
0.5
0.0
[Ab]
nM
33
8.25
2.06
ch9F7-F11
ch9F7-F11 Emb
H4B-121
H4B-121 Emb
B
ADCC lysis of MDA-MB453 cells (%)
w/o NRG1
with NRG1
80
60
40
20
0
[Ab]
nM
0.0066
0.066
0.66
6.6
Px
9F7-F11
ch9F7-F11 Emb
H4B-121
H4B-121 Emb

Fig.4

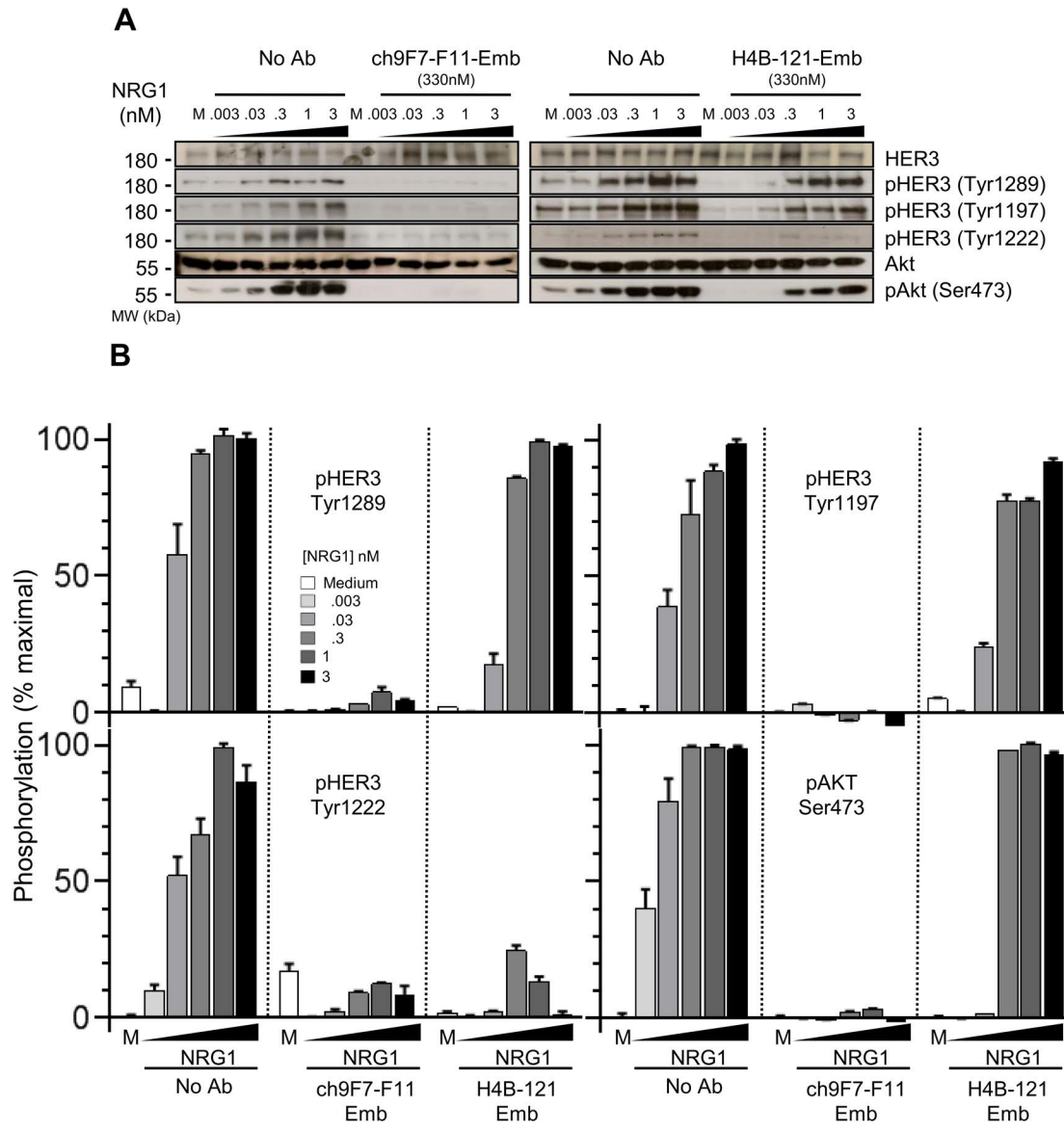
A
No Ab
ch9F7-F11-Emb
(330nM)
No Ab
H4B-121-Emb
(330nM)
NRG1
(nM)
M .003 .03 .3 1 3 M .003 .03 .3 1 3
M .003 .03 .3 1 3 M .003 .03 .3 1 3
180
180
180
180
55
55
MW (kDa)
HER3
pHER3 (Tyr1289)
pHER3 (Tyr1197)
pHER3 (Tyr1222)
Akt
pAkt (Ser473)
B
Phosphorylation (% maximal)
100
50
0
pHER3
Tyr1289
[NRG1] nM
Medium
.003
.03
.3
1
3
pHER3
Tyr1197
pHER3
Tyr1222
pAKT
Ser473
M
NRG1
No Ab
ch9F7-F11
Emb
H4B-121
Emb

Fig.5

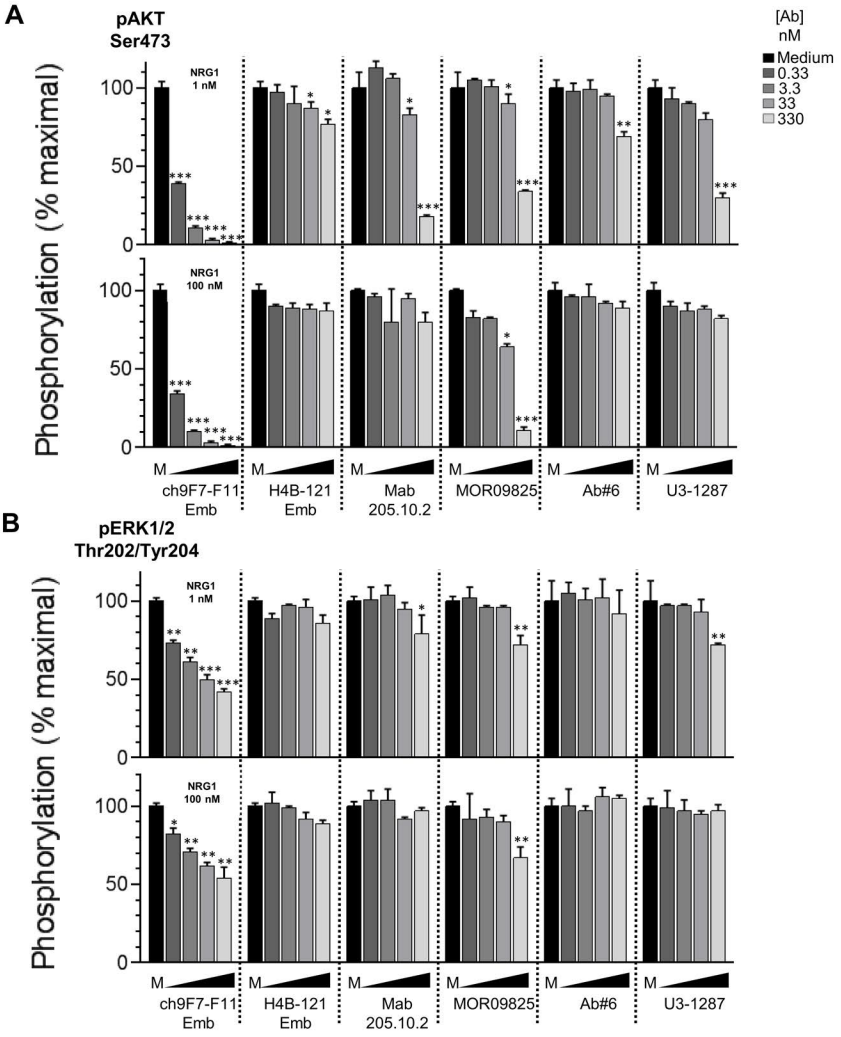
A
pAKT
Ser473
[Ab]
nM
Medium
0.33
3.3
33
330
NRG1
1 nM
NRG1
100 nM
Phosphorylation (% maximal)
M
ch9F7-F11
Emb
H4B-121
Emb
Mab
205.10.2
MOR09825
Ab#6
U3-1287
B
pERK1/2
Thr202/Tyr204

Fig.6

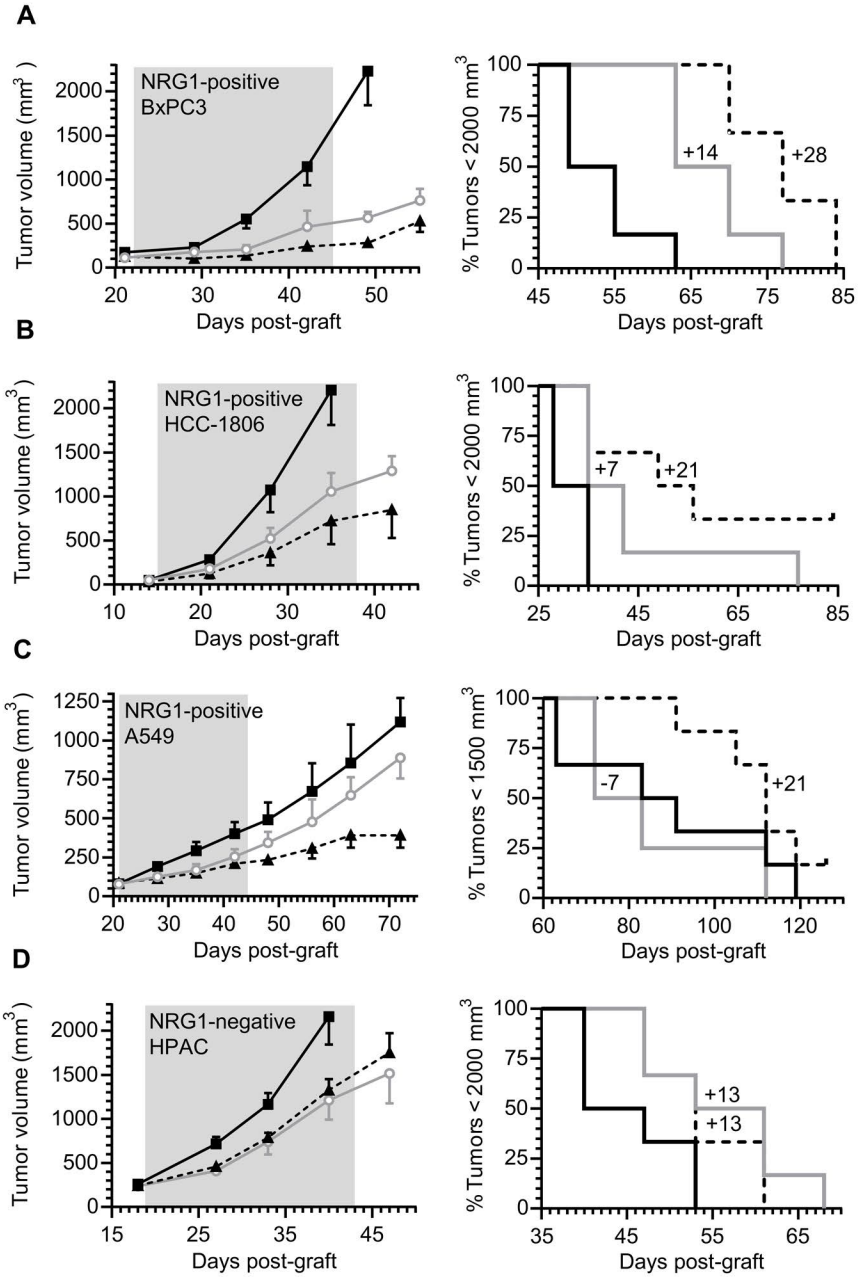
A
NRG1-positive
BxPC3
Tumor volume (mm3)
Days post-graft
% Tumors < 2000 mm3
+14
+28
B
NRG1-positive
HCC-1806
+7
+21
C
NRG1-positive
A549
% Tumors < 1500 mm3
-7
+21
D
NRG1-negative
HPAC
+13
+13